Non-hydrostatic modeling of drag, inertia and porous effects in wave propagation over dense vegetation fields

Suzuki, Tomohiro; Hu, Zhan; Kumada, Kenji; Phan Khanh, Linh; Zijlema, Marcel

DOI
10.1016/j.coastaleng.2019.03.011

Publication date
2019

Document Version
Final published version

Published in
Coastal Engineering

Citation (APA)
Suzuki, T., Hu, Z., Kumada, K., Phan Khanh, L., & Zijlema, M. (2019). Non-hydrostatic modeling of drag, inertia and porous effects in wave propagation over dense vegetation fields. *Coastal Engineering*, *149*, 49-64. https://doi.org/10.1016/j.coastaleng.2019.03.011

Coastal Engineering 149 (2019) 49–64

Contents lists available at ScienceDirect

Coastal Engineering

journal homepage: www.elsevier.com/locate/coastaleng

Non-hydrostatic modeling of drag, inertia and porous effects in wave propagation over dense vegetation fields

Tomohiro Suzuki[a,b], Zhan Hu[c,d,e,*], Kenji Kumada[f], L.K. Phan[b], Marcel Zijlema[b]

[a] Flanders Hydraulics Research, Berchemlei 115, 2140, Antwerp, Belgium
[b] Faculty of Civil Engineering and Geosciences, Delft University of Technology, Stevinweg 1, 2628, CN Delft, the Netherlands
[c] School of Marine Science, Sun Yat-sen University, Guangzhou, 510275, China
[d] Southern Laboratory of Ocean Science and Engineering (Guangdong, Zhuhai), Zhuhai, 519000, China
[e] Guangdong Provincial Key Laboratory of Marine Resources and Coastal Engineering, Guangzhou 510275, China
[f] Faculty Engineering Science, Katholieke Universiteit Leuven, Belgium

ARTICLE INFO

Keywords:
Wave-vegetation interaction
Horizontal vegetation cylinders
Porosity effect
Inertia force
Dense vegetation
SWASH model

ABSTRACT

A new wave-vegetation model is implemented in an open-source code, SWASH (Simulating WAves till SHore). The governing equations are the nonlinear shallow water equations, including non-hydrostatic pressure. Besides the commonly considered drag force induced by vertical vegetation cylinders, drag force induced by horizontal vegetation cylinders in complex mangrove root systems, as well as porosity and inertia effects, are included in the vegetation model, providing a logical supplement to the existing models. The vegetation model is tested against lab measurements and existing models. Good model performance is found in simulating wave height distribution and maximum water level in vegetation fields. The relevance of including the additional effects is demonstrated by illustrative model runs. We show that the difference between vertical and horizontal vegetation cylinders in wave dissipation is larger when exposed to shorter waves, because in these wave conditions the vertical component of orbital velocity is more prominent. Both porosity and inertia effects are more pronounced with higher vegetation density. Porosity effects can cause wave reflection and lead to reduced wave height in and behind vegetation fields, while inertia force leads to negative energy dissipation that reduces the wave-damping capacity of vegetation. Overall, the inclusion of both effects leads to greater wave reduction compared to common modeling practice that ignores these effects, but the maximum water level is increased due to porosity. With good model performance and extended functions, the new vegetation model in SWASH code is a solid advancement toward refined simulation of wave propagation over vegetation fields.

1. Introduction

Coastal wetlands, such as mangroves, saltmarshes and seagrasses, are now widely recognized as effective buffers to incident wave energy, even during storm conditions (Asano et al., 1988; Arkema et al., 2013; Möller et al., 2014). Initiatives have now been taken to integrate these natural or constructed wetlands into overall coastal-protection schemes to mitigate wave impacts and associated erosion (Borsje et al., 2011; Temmerman et al., 2013). One example is the “Building with Nature” approach originated in the Netherlands, which includes natural wetlands in the infrastructure designs for improved flexibility and ecosystem services (Borsje et al., 2011; Cuc et al., 2015; de Vriend et al., 2015).

To design the required wetland space for wave dampening, quantitative assessment of the efficiency of wave damping by vegetation is needed (Bouma et al., 2014). Furthermore, besides wave energy dissipation, other wave propagation processes in vegetation wetlands, such as wave reflection and diffraction, should be properly quantified, since wave fields as a whole may have important impacts on an ecosystem's initial establishment and long-term health (Mariotti and Fagherazzi, 2010; Balke et al., 2011; Hu et al., 2015).

With continuous development, numerical models are becoming valuable tools to estimate wave propagation over coastal wetlands under various scenarios (Borsje et al., 2011; Mei et al., 2011; Suzuki et al., 2012; Liu et al., 2015; van Loon-Steensma et al., 2016). Several models that quantify the effect and process of wave propagation through vegetation fields are listed in Table 1. These models are categorized into two groups based on their controlling physical equations: energy-conservation models and momentum-conservation models. In the first group, wave dissipation by vegetation was initially modeled as

* Corresponding author. No. 135, Xingang Xi Road, Guangzhou, 510275, China.
E-mail address: huzh9@mail.sysu.edu.cn (Z. Hu).

https://doi.org/10.1016/j.coastaleng.2019.03.011
Received 8 August 2017; Received in revised form 31 January 2019; Accepted 26 March 2019
Available online 29 March 2019
0378-3839/

Table 1
A review of wave-vegetation interaction models.

Source	Control equation	Vegetation schematization	Temporal resolution	Incident wave condition	Drag by horizontal vegetation cylinders	Porosity	Inertia force	Computation cost
Hasselmann and Collins (1968); Möller et al. (1999)	Energy conservation equation	Bottom friction	Phase-averaging	Regular waves	No	No	No	Low
Dalrymple et al. (1984); Losada et al. (2016); Méndez and Losada (2004);	Energy flux conservation equation	Rigid/fixable cylinders	Phase-averaging	Regular/ irregular waves	No	No	No	Low
Suzuki et al. (2012)	Spectral action balance equation	Rigid cylinders	Phase-averaging	Regular/ irregular waves	No	No	No	Low
Cao et al. (2015); Tang et al. (2015)	Mild-slope equation	Rigid cylinders	Phase-averaging/phase-resolving	Regular/ irregular waves	No	No	No	Low
Kobayashi et al. (1993); Méndez et al. (1999); Mei et al. (2011); Liu et al. (2015)	Shallow water equations	Rigid/fixable cylinders	Phase-averaging/phase-resolving	Regular/ irregular waves	No	No	No	Low
Augustin et al. (2009); Huang et al. (2011); Iimura and Tanaka (2012); Karambas et al. (2016); Yang et al. (2018)	Boussinesq equations	Rigid cylinders	Phase-resolving	Regular/ irregular waves	No	No/Yes	No/Yes	Medium
Li and Yan (2007); Ma et al. (2013); Maza et al. (2013); Chen et al. (2016); Maza et al. (2015, 2016)	RANS equations	Rigid/fixable cylinders	Phase-resolving	Regular/ irregular waves	No	No	No	High
van Rooijen et al. (2016)	Wave action balance equation (for short waves) + nonlinear shallow water equations (for long waves)	Rigid cylinders	Envelop-resolving + phase-resolving	Irregular waves	No	No	No	Low
Present study	Nonlinear shallow water equations	Rigid cylinders	Phase-resolving	Regular/ irregular waves	Yes	Yes	Yes	Medium

added bottom friction (Hasselmann and Collins, 1968; Möller et al., 1999). Dalrymple et al. (1984) introduced a theoretical model that accounts for wave dissipation by vertical vegetation cylinders over the water column following linear wave theory. In this model, the wave dissipation in vegetation canopies is attributed to the drag force exerted by vegetation stems expressed by Morison equations (Morison et al., 1950). Several parameters describing vegetation canopies, such as number of vegetation stems in a unit area, stem diameter, and vegetation height, can be accounted for explicitly. Thus, the process of wave dissipation by vegetation can be quantified in detail. More recent work has modified the original model of Dalrymple et al. (1984) to incorporate the effect of wave breaking, wave irregularity and wave-current interaction (Méndez and Losada, 2004; Losada et al., 2016). Among energy-conservation models, the effect of wave dissipation by vegetation has also been introduced to a spectral-action balance equation model (Suzuki et al., 2012) and mild-slope equation models (Tang et al., 2015; Cao et al., 2015).

Momentum-conservation models seek to simulate wave propagation through vegetation by quantifying vegetation-induced momentum lost. The applied equations in these models include shallow water equations, Boussinesq-type equations, and Reynolds-averaged Navier-Stokes (RANS) equations (Table 1). As these equations are all based on momentum conservation, these models can provide not only wave-field information but also velocity structures with intra-wave (phase-resolving) resolutions, which is important for interpreting both wave propagation and sediment transport processes in coastal wetlands. Because of the increased scope and resolutions, these models are generally expensive in terms of computation time comparing to wave-energy conservation models.

Reviewing the previous work listed in Table 1, it becomes clear that drag force induced by horizontal vegetation stems/roots, inertia force, and porosity are often neglected in numerical models. Existing models often only consider vegetation structures as vertical cylinders, but natural vegetation systems such as mangroves have complex root systems composed of both vertical and horizontal roots (Ohira et al., 2013; Kamal et al., 2014) (Fig. 1a and b). Additionally, horizontal vegetation stems are seen in recent innovative coastal-protection projects that apply porous brushwood groins for wave damping and mangrove nurseries, e.g., in “Build with Nature, Indonesia” (Lucas, 2017). The force acting on horizontal vegetation cylinders has both horizontal and vertical components, whereas the latter is generally neglected in existing models that deal with only vertical vegetation cylinders (Fig. 2). The force on the horizontal vegetation stems/roots and the associated wave-energy dissipation need to be further investigated both theoretically and numerically.

Besides drag force, inertia force is the other component in the total force that acts on vegetation (Morison et al., 1950; Chen et al., 2018; Yao et al., 2018). Inertia force is commonly ignored in wave-vegetation modeling because the work done by the theoretical inertia force over one wave cycle is zero if linear wave theory is applied. However, coastal wetlands are normally located in shallow intertidal areas, where wave nonlinearity exists. For nonlinear waves, the work done by inertia force is nonzero. The effect of inertia on wave dissipation can be of greater importance in the case of dense vegetation with lower porosities, as inertia force is proportional to the spatial occupation of vegetation per unit volume (i.e., $\phi = N_v(\pi/4)b_v^2$, where N_v and b_v are the number of plants per square meter and the stem diameter, respectively). The value of ϕ can be as high as 0.45 in natural mangroves and even 0.65 in constructed coastal wetlands (Furukawa et al., 1997; Mazda et al., 1997; Serra et al., 2004). Thus, the inertia effect in these high-density conditions is potentially important in wave-propagation modeling, and is worthy of detailed investigation.

Also commonly ignored is the porosity effect, which is induced by the existence of vegetation in the water column that can “squeeze” the flow passing through it, leading to higher in-canopy velocity and influencing wave propagation through the vegetation field (Mei et al., 2011; Liu et al., 2015). The inclusion of the porosity effect can lead to possible reflection in wave-vegetation models ((Arnaud et al., 2017)), which contributes to wave-height reduction behind the vegetation. The porosity effect is relevant in dense mangrove fields (e.g., Fig. 1a), and also in porous brushwood groins made up of dense wooden sticks (Lucas, 2017). Vegetation density can be expressed by the frontal vegetation area per canopy volume (i.e., $N_v * b_v$) or by canopy porosity (n = 1-ϕ) (Nepf, 2011). However, with the same value of $N_v * b_v$, porosity can be different, which may considerably influence wave propagation through vegetation fields.

In this paper, a new vegetation model is developed in the time-domain wave-modeling code SWASH (Zijlema et al., 2011). Besides the commonly considered drag force induced by vertical vegetation cylinders, the vegetation model also includes horizontal vegetation cylinders and the effects of porosity and inertia, providing a logical supplement to existing studies (see Table 1). SWASH is a general-purpose numerical tool for simulating unsteady, non-hydrostatic, and free-surface flow phenomena in coastal waters. It is chosen to implement a vegetation model because of its open-source nature and its efficiency in handling large 2D computational domains. In section 2, we introduce the vegetation model and implementation in SWASH. In addition, we present a theoretical model that handles wave damping by horizontal vegetation cylinders. In section 3, we focus on testing the implementation of drag force induced by both vertical and horizontal vegetation cylinders. Modeled wave dissipation by vertical vegetation cylinders is evaluated against measurements and existing models. The difference between

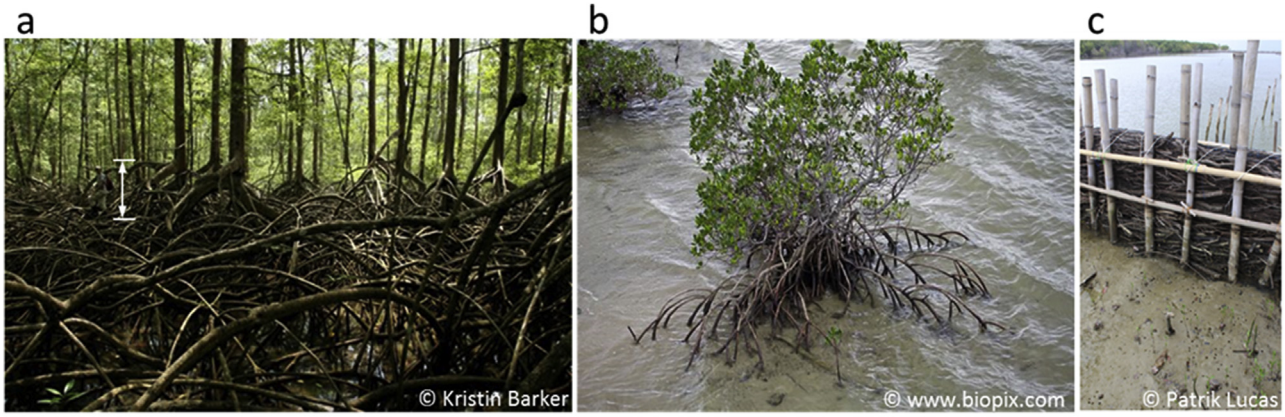

Fig. 1. (a) An example of a mangrove forest with complex, high-density roots, which is a mixture of h4orizontal and vertical cylinders. The scale in the photo shows a standing person; (b) wave propagation through horizontal and vertical mangrove roots; (c) permeable brushwood groin with horizontal wooden sticks for wave dampening, and a mangrove nursery.

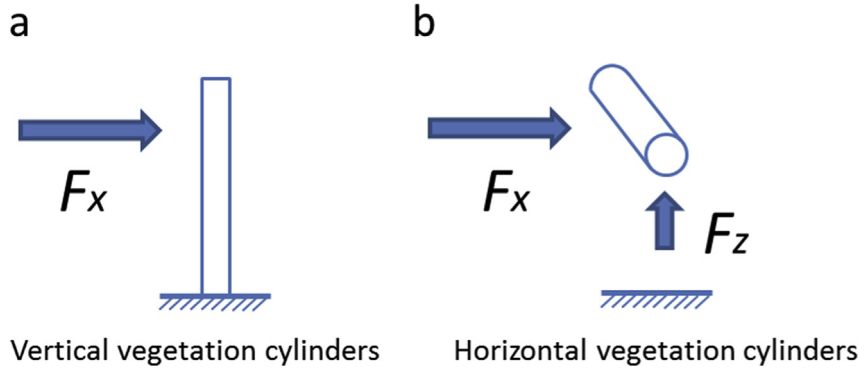

Fig. 2. (a) Schematization of the force acting on vertical vegetation cylinders; (b) Schematization of the force acting on horizontal vegetation cylinders, which has both horizontal and vertical components.

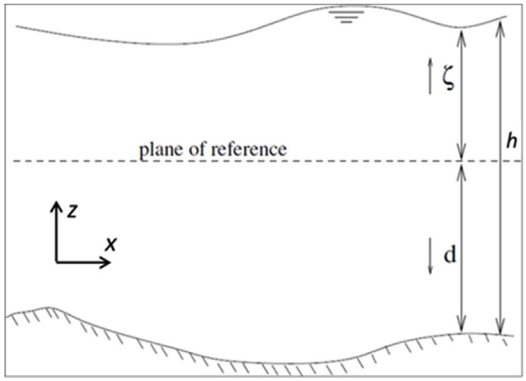

Fig. 3. Water area with bottom and free surface.

vertical and horizontal vegetation cylinders in wave dissipation is identified by modeling. In section 4, we test the inclusion of the porosity effect against lab experimental data, and explore how porosity and inertia effects can affect wave transmission over vegetation patches. Finally, in section 5, we discuss the overall model performance, the influence of the included effects, and potential coastal-management implications and applications.

2. Model

2.1. Governing equations

The SWASH model is a time-domain model for simulating non-hydrostatic, free-surface, and rotational flow. The governing equations are the shallow water equations, including a non-hydrostatic pressure term. We consider a two-dimensional domain that is bounded vertically by a free surface $z = \zeta(x,t)$ and a fixed bed $z = -d(x)$ (see Fig. 1). Here t is time, x and z are the Cartesian coordinates, and $z = 0$ is the still-water level. The governing equations are:

$$\frac{\partial u}{\partial x} + \frac{\partial w}{\partial z} = 0 \tag{1}$$

$$\frac{\partial u}{\partial t} + \frac{\partial uu}{\partial x} + \frac{\partial wu}{\partial z} = -g\frac{\partial \zeta}{\partial x} - \frac{\partial q}{\partial x} - \frac{1}{\rho}F_x \tag{2}$$

$$\frac{\partial w}{\partial t} + \frac{\partial uw}{\partial x} + \frac{\partial ww}{\partial z} = -\frac{\partial q}{\partial z} - \frac{1}{\rho}F_z \tag{3}$$

where $u(x, z, t)$ is the velocity in the x direction, $w(x, z, t)$ is the velocity in the z direction, g is the gravitational acceleration, ρ is the water density, $q(x, z, t)$ is the non-hydrostatic pressure (normalized by density ρ), and F_x and F_z represent body and surface forces in the x and z direction, respectively, e.g., Coriolis force, atmospheric and baroclinic pressure gradients, and gradients of turbulent stresses. We will not consider these forces. Instead, we will consider forces acting on vegetation cylinders; see Section 2.2.

At the free surface and bottom levels, the following kinematic boundary conditions apply:

$$w|_{z=\zeta} = \frac{\partial \zeta}{\partial t} + u\frac{\partial \zeta}{\partial x} \tag{4}$$

$$w|_{z=-d} = -u\frac{\partial d}{\partial x} \tag{5}$$

To close the set of equations, we derive an extra equation to determine the free surface elevation ζ. Integrating the continuity equation (1) from the bottom to the free surface and applying the relevant kinematic boundary conditions (4) and (5) yield the following global continuity equation:

$$\frac{\partial \zeta}{\partial t} + \frac{\partial hu}{\partial x} = 0 \tag{6}$$

where $h = \zeta + d$ is the water depth (see Fig. 3).

A full description of the numerical model, boundary conditions, numerical approach, and applications is given in Zijlema et al. (2011).

2.2. Vegetation model

Form drag and inertia force in the Morison equation are among the key elements in the modeling of vegetation. The horizontal component of the form drag and inertia force acting on the vegetation per unit volume can be described as follows:

$$F_x = \frac{1}{2}\rho C_D h_v b_v N_v u|u| + \rho(1 + C_m)h_v A_v N_v \frac{du}{dt} \tag{7}$$

where C_D is a bulk drag coefficient, h_v is the cylinder height, b_v is the stem diameter of the cylinder (plant), N_v is the number of plants per square meter, u is the horizontal velocity due to wave motion, C_m is the added-mass coefficient, and A_v is the area of a single cylinder, i.e.,

$$A_v = \frac{\pi}{4}b_v^2 \tag{8}$$

In this study, stiff vegetation is modeled as a group of rigid circular cylinders for simplicity. When cylinders are vertical, only the drag force in the horizontal direction (Fx) is considered (Fig. 2). When cylinders are horizontal (e.g., box filled with branches), the forces in both the horizontal and vertical directions (Fx and Fz) are considered. The vertical drag force is:

$$F_z = \frac{1}{2}\rho C_D h_v b_v N_v w|w| \tag{9}$$

Vertical inertia force and vegetation surface friction are neglected, seeing that form drag is dominant in the tested cases. Swaying motion

and vibration due to vortices are also neglected, as these cylinders are assumed to be rigid.

In addition to the drag and inertia terms, porosity is considered in the vegetation model in this work. The interface of the vegetation would influence the wave propagation, especially in a densely populated vegetated area. The porosity effect is modeled by considering the pore velocity as the characteristic velocity instead of the mean flow (Burcharth and Andersen, 1995; Jensen et al., 2014). The pore velocity is defined as

$$u_p = \frac{u}{n} \tag{10}$$

where n is porosity, which is the ratio of the fluid volume to the total volume. In this context, u is the filter (or spatially-averaged) velocity (for details, see Jensen et al. (2014)).

2.3. Implementation of vegetation model in SWASH

Drag and inertia force, as represented in Eq. (7), are implemented in Eq. (2) as follows:

$$\left(1 - \frac{h_v}{h}\frac{\pi}{4}b_v^2 N_v\right)\frac{\partial u}{\partial t} + \frac{\partial uu}{\partial x} + \frac{\partial wu}{\partial z} + g\frac{\partial \zeta}{\partial x} + \frac{\partial q}{\partial x} + \frac{1}{2}C_D\frac{h_v}{h}b_v N_v u|u| + (C_m + 1)\frac{h_v}{h}\frac{\pi}{4}b_v^2 N_v\frac{\partial u}{\partial t} = 0 \tag{11}$$

Note that the first term in the left-hand side of Eq. (11) is considered as the inertia term acting onto the clear fluid, whereas the last term is the inertia force associated with the displaced volume of water due to vegetation. Substituting $(1 - n) = \frac{h_v}{h}\frac{\pi}{4}b_v^2 N_v$, we obtain

$$\{1 + C_m(1 - n)\}\frac{\partial u}{\partial t} + \frac{\partial uu}{\partial x} + \frac{\partial wu}{\partial z} + g\frac{\partial \zeta}{\partial x} + \frac{\partial q}{\partial x} + \frac{1}{2}C_D\frac{h_v}{h}b_v N_v u|u| = 0 \tag{12}$$

To include porosity effects the ambient flow in porous media is characterized by the pore velocity (Burcharth and Andersen, 1995). In addition, both advection and pressure gradient are acting onto the clear fluid (Jensen et al., 2014). The momentum equation for the porous media is obtained as follows:

$$\{1 + C_m(1 - n)\}\frac{\partial\left(\frac{u}{n}\right)}{\partial t} + n\frac{\partial\left(\frac{u}{n}\right)^2}{\partial x} + n\left(g\frac{\partial \zeta}{\partial x} + \frac{\partial q}{\partial x}\right) + \frac{1}{2}C_D\frac{h_v}{h}b_v N_v\frac{u}{n}\left|\frac{u}{n}\right| = 0 \tag{13}$$

This momentum equation and the continuity equation, given by Eq. (6), are the governing equations for the vegetation flow modeling to be applied in this study. Note that velocity u in Eq. (6) is the filter velocity (Jensen et al., 2014).

3. Validation of drag force implementation of vertical and horizontal vegetation cylinders

As drag force contributes the bulk of wave dissipation, we first tested the drag force-oriented wave dissipation. Cases with vertical (sections 3.1, 3.2, and 3.3) and horizontal (section 3.4) vegetation cylinders were both explored. The tests with vertical cylinders included comparisons against classic analytical models as well as lab measurements. To obtain a comprehensive validation, both flat and sloping beds as well as 1D and 2D modeling runs are presented. The SWASH model tests in this paper were ran with more than 200 waves to obtain constant wave fields suggested by Goda (2010).

3.1. One-dimensional wave propagation over vertical vegetation on a flat bottom

Comparison with existing theoretical models can be a good benchmark for the new model. In this section, the present model was compared with the model of Méndez and Losada (2004) for validation. The latter is a classic analytical model that deals with wave dissipation over vertical vegetation, and is included in the appendix. The model runs were taken in 1DH. The total length of the computational grid was set as 150 m, with a grid size of 0.5 m. The test waves were unidirectional non-breaking random waves, with significant wave height at the boundary being 0.2 m. For all runs, the JONSWAP spectrum was used with the peak enhancement factor $\gamma = 3.3$. The tested peak wave period (T_p) was 4 s, 6 s, 10 s, and 20 s, and the water depth was 3.0 m. Thus, the kh values of these tests were 0.99, 0.61, 0.35, and 0.17, respectively, where k is the wave number. Both the initial water level and velocity components were set to zero, and the bottom friction was neglected. The vegetation parameters b_v, C_D, and N_v were 0.01 m, 1.0, and 100, respectively. The C_D value is chosen to simplify model comparison. Both emerged and submerged vegetation conditions were included. The vegetation height was 5 m for the emergent-vegetation case and 1 m for submerged vegetation.

3.1.1. Emergent vegetation

We first compared the vegetation model in SWASH and the Méndez and Losada (2004) model in the case of emergent vegetation. For such cases, only one vertical layer was used in SWASH. For all tested periods, the wave period reduced gradually in the vegetation field (x = 0–150, Fig. 4). Good agreement was found between these two models in terms of wave dissipation. Thus, the same wave attenuation as in the random wave transformation model can be obtained using the vegetation model in SWASH.

3.1.2. Submerged vegetation

We further tested the vegetation model in SWASH against the model of Méndez and Losada (2004) under the condition of submerged vegetation. To test the effect of including more vertical layers in SWASH simulation, the model runs were conducted using both one and two vertical layers. As can be seen from Fig. 5, all the cases with one vertical layer, except for $T_p = 4$ s, show good agreement with the analytic model. When the wave is short (i.e., large kh), the one-layer model is not suitable in simulating wave transformation over a submerged vegetation field. This is because the horizontal velocity profile is not uniform in cases of short waves, the one-layer model can only provide a uniform velocity profile, and it uses this depth-averaged velocity in the calculation of wave dissipation. This leads to overestimation of the velocity acting on submerged vegetation, since submerged vegetation is close to the bed with lower velocity than the depth-averaged velocity. The overestimation of velocity leads to magnified wave attenuation (Fig. 5). When waves are longer, velocity profiles become more uniform. The difference between the actual and modeled velocity profiles is reduced, which leads to more accurate wave-height calculation. To overcome the limitation with one-layer modeling, two or more vertical layers can be used in SWASH, which shows a better fit to the theoretical value in the case of short waves.

3.2. One-dimensional wave propagation over vertical vegetation on a slope

The new model was further validated against the data from the physical model reported by Wu et al. (2011). In their physical model, the vegetation patch was placed on a sloping bed (lower panel of Fig. 6). The tested C_D, b_v, N_v, h_v, and water depth were 1.7, 0.0032, 3182, 0.2, and 0.69 respectively. The C_D was determined by calibration. Its value is reasonable as it is in the common range reported in the literature (Nepf, 2011). The tested vegetation mimics are rigid. The tested waves were random, unidirectional waves. The incident significant wave height was 0.06 m, with a peak wave period of 2.4 s. For better demonstration, both cases with and without vegetation were included in the tests. In the case without vegetation, the modeled wave was almost uniform in space until x = 13 m, where waves started to break on the slope until the wave height went to zero (Fig. 6a). This

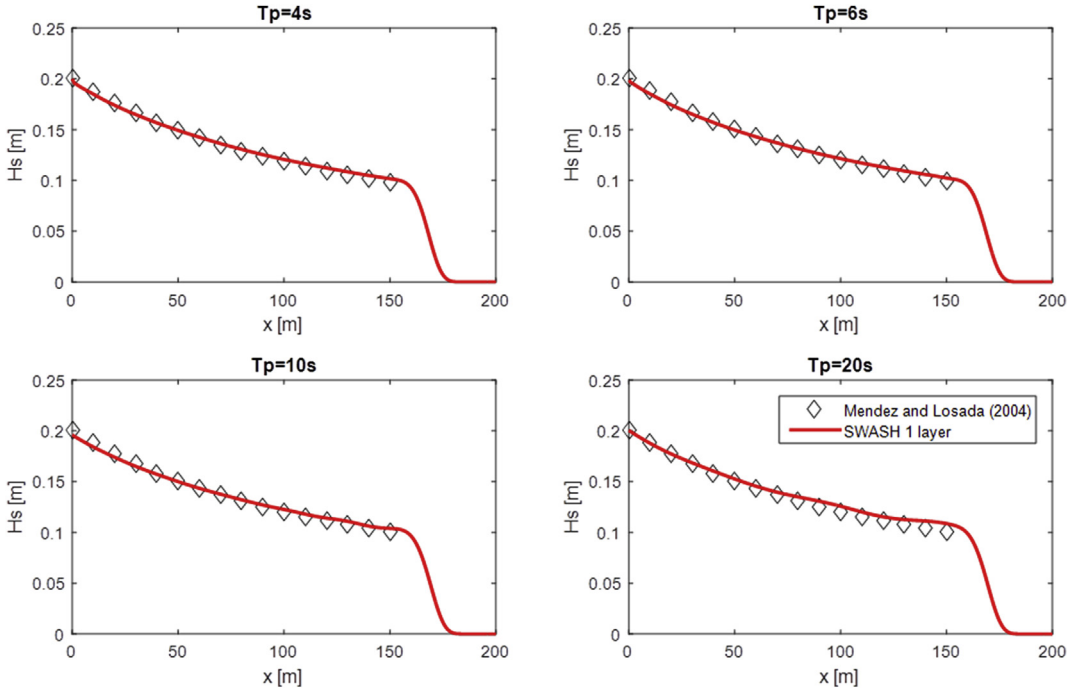

Fig. 4. Modeled spatial distribution of H_s in emergent vegetation field. The vegetation field is from x = 0–150 m. *Tp* of the incident wave period is 4–20 s. Only one vertical layer is applied in the SWASH model. A sponge layer is applied at the end of the domain (x = 150–200) to avoid wave reflection.

result agrees well with the physical model. For the case with vegetation, the gentle wave breaking on the slope was replaced by a rapid wave-height reduction induced by vegetation. It is also apparent that the SWASH model agrees very well with the physical model. Specifically, the small increase of wave height near the vegetation front (x = 11.7 m) is well captured by the SWASH model, which shows that the model can provide detailed and accurate wave-height simulation.

3.3. Two-dimensional wave propagation over patchy vertical vegetation on a slope

In this section, we examine the performance of the SWASH vegetation model in 2DH. The model was compared to the SWAN model results reported in Cao et al. (2015). The model configuration represented a coastline with patchy vegetation clumps (Fig. 7a). The tested C_D, b_v, N_v, and h_v were 0.5, 0.01 m, 100 stems/m^2, and 3 m, respectively. The C_D value is chosen to follow the original model setup

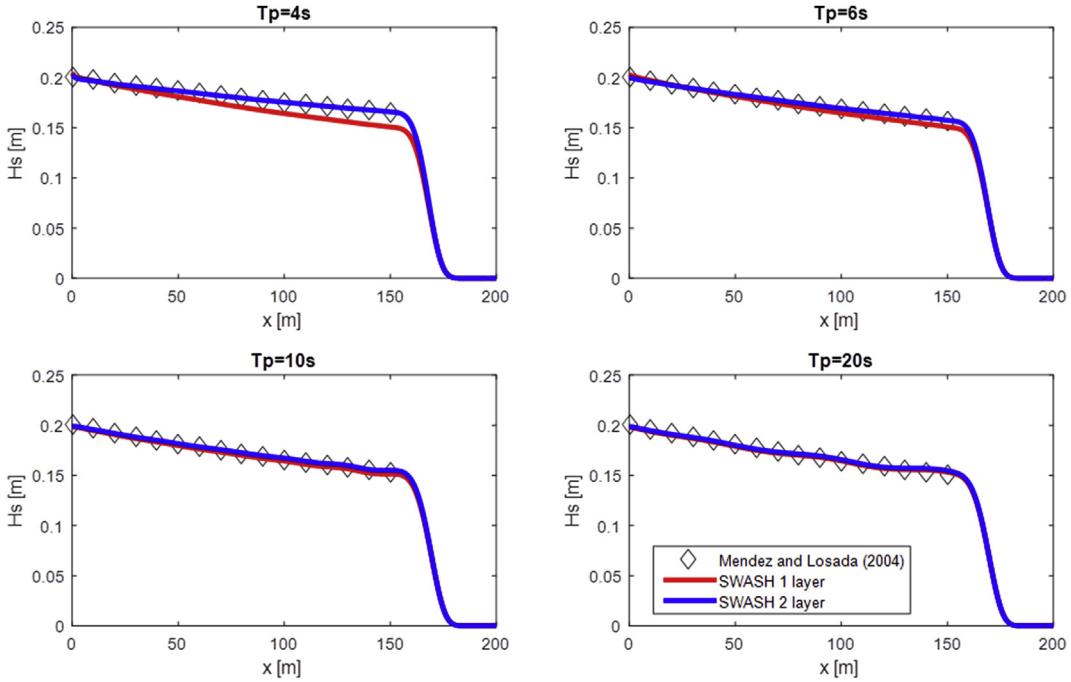

Fig. 5. Modeled spatial distribution of H_s in submerged vegetation field. The vegetation field is from x = 0–150 m. *Tp* of the incident wave period is 4–20s. One and two vertical layers are applied in the SWASH model. A sponge layer is applied at the end of the domain (x = 150–200) to avoid wave reflection.

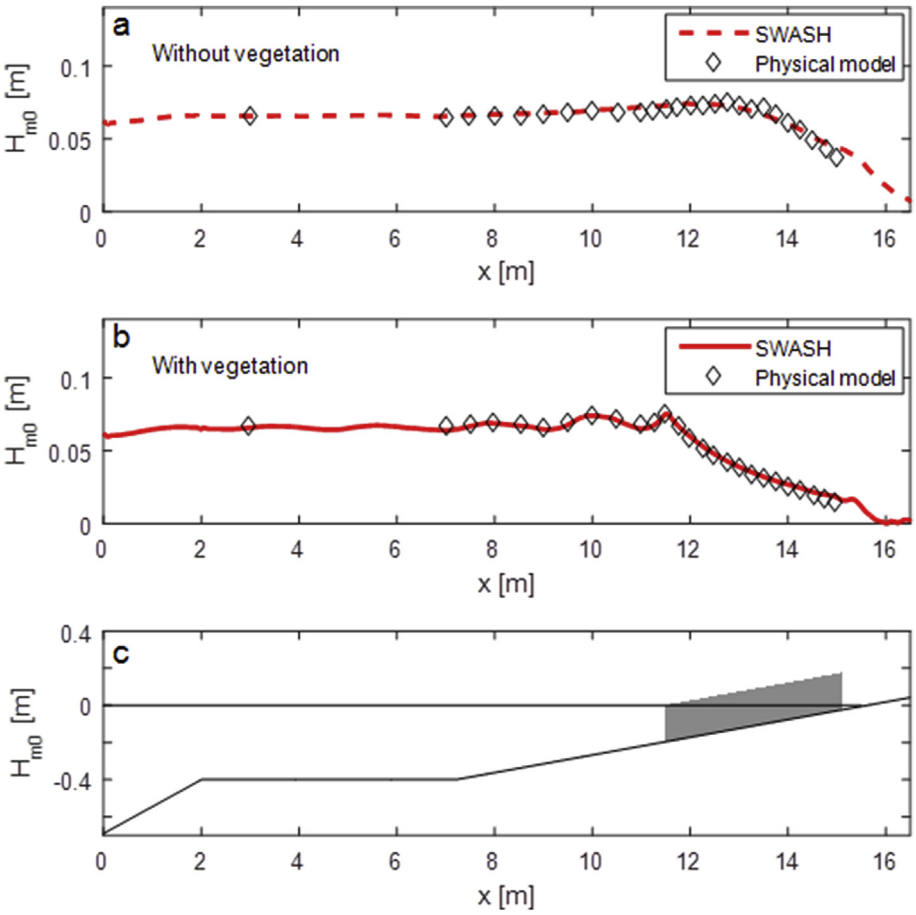

Fig. 6. Comparison between the modeled and measured wave-height distribution without and with a vegetation patch (panels a and b). The experiment setup is shown in panel c with a vegetation patch on a sloping bed at x = 11.7 m–15 m.

in Cao et al. (2015). The computation domain was a slope on which the water depth was in the range of 0–5 m, and the vegetation was always emergent (Fig. 7a). The tested H_s was 1 m, and T_p was 3.5 s. The tested waves were unidirectional random waves, which were perpendicular to the x-direction. To facilitate the 2DH model comparison, six transects were marked in the model domain, along which the simulated wave height could be compared. These transects were either long-shore or cross-shore, and they were placed inside as well as between vegetation patches to insure a comprehensive representation of the wave field.

Based on the wave-height comparison along each transect, the SWASH model results are qualitatively similar to the results generated by the SWAN model (Figs. 7 and 8). The overall agreement between these two models is good, except for some small differences between and behind vegetation patches. It is likely because phase-resolving models like SWASH handle diffraction effects better than phase-averaged models like SWAN (Cao et al., 2015).

3.4. One-dimensional wave propagation over horizontal cylinders

To compare wave dissipation by vertical and horizontal vegetation cylinders, both theoretical and SWASH modeling are presented. For the tests with vertical vegetation cylinders, the classic theoretical model in Méndez and Losada (2004) was applied. For the case with horizontal vegetation, the theoretical wave dissipation model was extended to include the vertical drag force (*Fz*) on vegetation:

$$H_{rms} = \frac{H_{rms,o}}{1 + \beta x} \tag{14a}$$

and

$$\tilde{\beta} = \frac{1}{3\sqrt{\pi}} C_D b_v N_v H_{rms,o} k \frac{\sinh^3(k\alpha d) + 3\sinh(k\alpha d) + \cosh^3(k\alpha d) - 3\cosh(k\alpha d) + 2}{\{\sinh^2(2kd) + 2kd\}\sinh(kd)} \tag{14b}$$

Details of the theoretical models for vertical and horizontal vegetation cylinders are included in the appendix.

For the hydrodynamic conditions, the tested H_s, h, and T_p were 0.2 m, 3 m, and 3–10 s, respectively. The tested vegetation parameters C_D, b_v, and N_v (in this case density per unit vertical area) were 1.0, 0.01 m, and 100 stems/m^2, respectively. This C_D value is chosen to facilitate simple model comparison. The height of the vertical vegetation cylinders or the wall of horizontal vegetation cylinders was 5.0 m to ensure vegetation-emergent conditions in all cases. Good agreement can be found between the SWASH model and the theoretical models (Fig. 9). It shows the competence of SWASH in modeling both vertical and horizontal vegetation cylinders. Furthermore, it is noticed that the difference in the H_s distribution between vertical and horizontal vegetation cylinders is more apparent in cases with shorter wave periods (e.g., T_p = 3 s), and the difference becomes smaller as the wave period increases. This is logical, as in shorter waves the ratio between the vertical orbital velocity (and vertical force *Fz*) to the horizontal orbital velocity (and horizontal force *Fx*) is larger, in which case the difference of including vertical force (*Fz*) is greater.

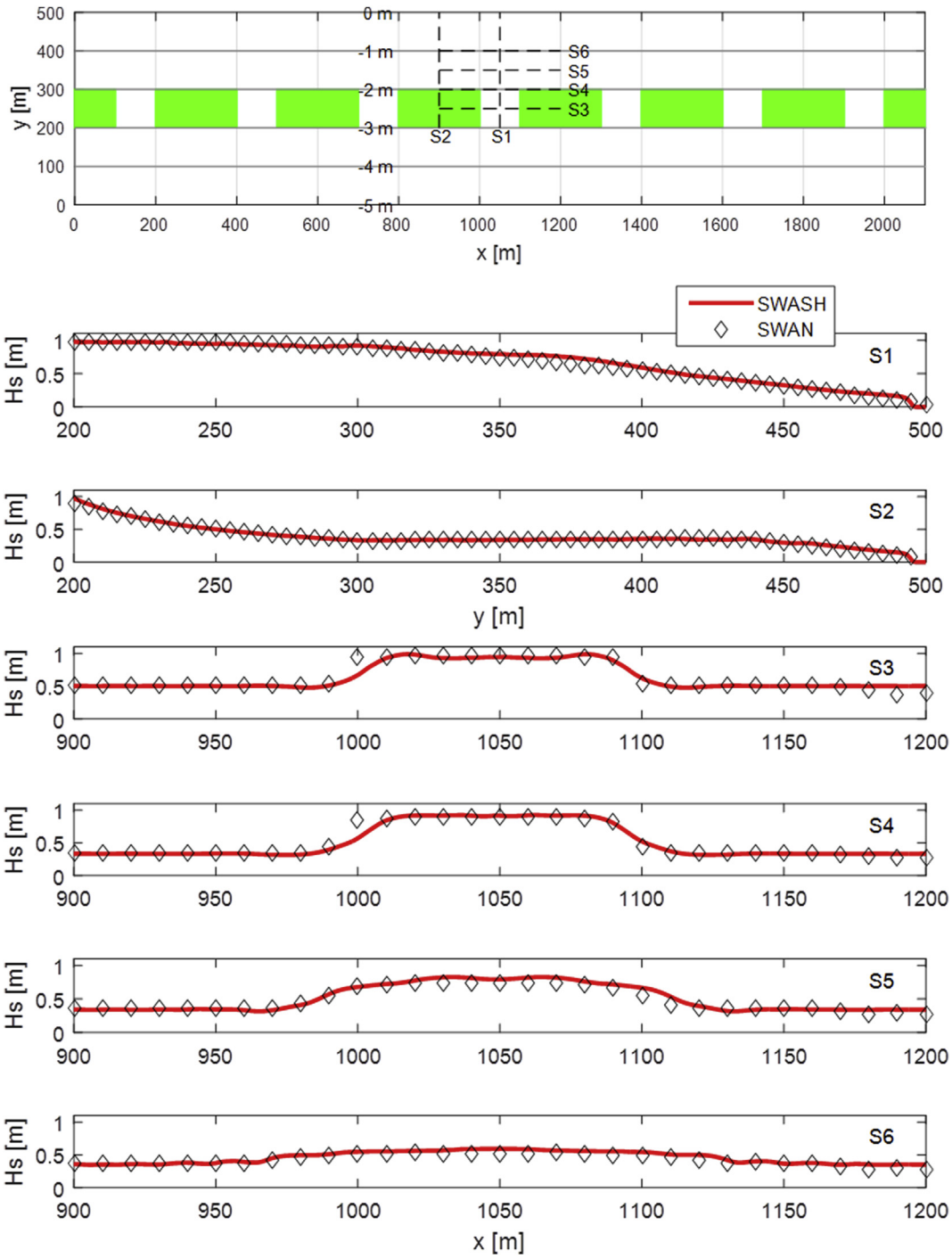

Fig. 7. Wave propagation over patchy vegetation. The tested waves are unidirectional random waves in the y direction. (a) Patchy vegetation on a slope. The elevation of the slope ranges from −5 m to 0 m, as indicated by the numbers near the contours. Six transects (S1−S6) are denoted by the dashed lines. Panels b–g show the modeling results along these transects obtained by both SWASH and SWAN models.

4. Porosity and inertia effects

4.1. Porosity and inertia effects in a solitary wave

In this section, we focus on validating the implementation of the porosity effect in the SWASH model. The solitary wave propagation in the physical model of Iimura and Tanaka (2012) is reproduced (Fig. 10d). The modeled maximum water level was compared against their measurement. In their physical model, the tested vegetation was always emergent. Three different stem densities were included: N_v= 462, 1283 and 11,547 stems/m^2 in cases 1 to 3, respectively. As the tested b_v was 0.005 m, spatial occupation of vegetation per unit volume ϕ was 0.009, 0.025, and 0.226 in these cases. With the increase of stem density, the length of the vegetation patch in the wave-propagation direction was reduced from 1 m to 0.04 m (Fig. 10a–c). To better capture wave transmission two layers were employed for case 3. The other two cases were ran with one layer. The tested waves were solitary waves. The C_D used in the simulation were 0.71, 0.66 and 1.73, respectively as given by Iimura and Tanaka (2012).

For cases 1 and 2 with relatively high porosity (i.e., low ϕ), the results with or without the porosity effect are very similar, and both agreed well with the measurement (Fig. 10a and b). In case 3, however,

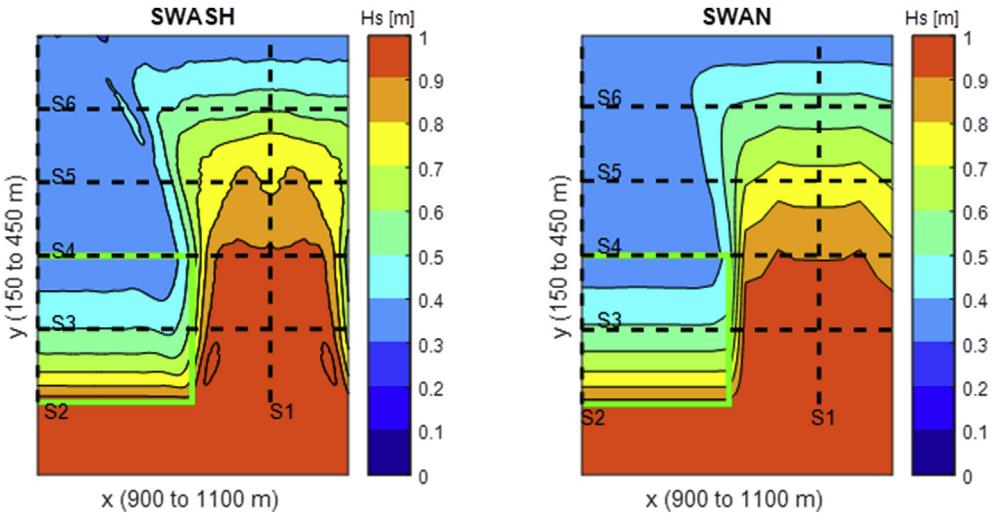

Fig. 8. Spatial distribution of H_s modeled by SWASH and SWAN in 2D. The setup of the computation domain is shown in Fig. 7a. The vegetation patch is indicated by a green rectangle. (For interpretation of the references to colour in this figure legend, the reader is referred to the Web version of this article.)

the low porosity (i.e., high ϕ) led to large local increases of maximum water level at the vegetation front due to wave reflection (Fig. 10c). This sharp increase was better captured by the runs with the porosity effect. It implies that in a dense vegetation field with low porosity, the maximum water level can be underestimated if the porosity effect is excluded. It is noted that the influence of inertia effect is limited when $Cm = 1$ is applied.

4.2. Porosity and inertia effects in regular and irregular waves

In this section, we demonstrate the effects of porosity and inertia in wave transformation by SWASH modeling, which were generally neglected in previous numerical investigations. We firstly compare the SWASH model with a flume experiment conducted in the Fluid Mechanics Laboratory at Delft University of Technology. Subsequently, we use the SWASH model to explore the porosity and inertia effects on wave transformation in vegetation canopies.

The setup of the flume experiment is shown in Fig. 11c. The mimicked vegetation canopy was constructed by wooden sticks with a diameter of 0.012 m. The first 0.5 m of the canopy has a higher density (porosity = 0.83) and the rest of the canopy has a lower density (porosity = 0.96). The tested water depth in the vegetation area was 0.3 m. The regular wave case has a wave height of 12 cm and a wave period of 2 s. C_D is calibrated as 1.7 for regular waves and 1.0 for irregular waves. These C_D values are calibrated based on the simulation without either porosity or inertia effect. They are subsequently applied to all the simulation cases. These values are reasonable since they are in the order of 1 as commonly reported in the literature (Nepf, 2011). The results

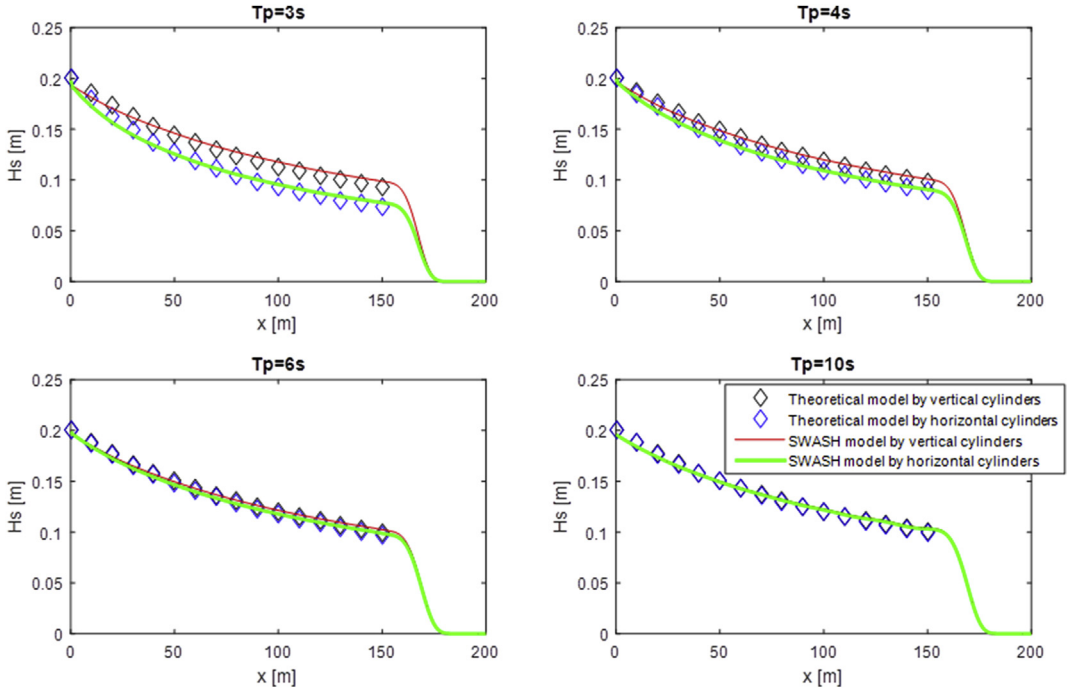

Fig. 9. Spatial distribution of H_s in a vegetation field with vertical or horizontal vegetation cylinders. The vegetation field is from x = 0–150 m. *Tp* of the incident wave period is 3–10s. Both theoretical and SWASH model results are included. For tests with vertical vegetation cylinders, the classic theoretical model in Méndez and Losada (2004) is applied. For tests with horizontal vegetation cylinders, an extended theoretical model is applied. Details of both models are included in Appendix. A sponge layer is applied at the end of the domain (x = 150–200) to avoid wave reflection.

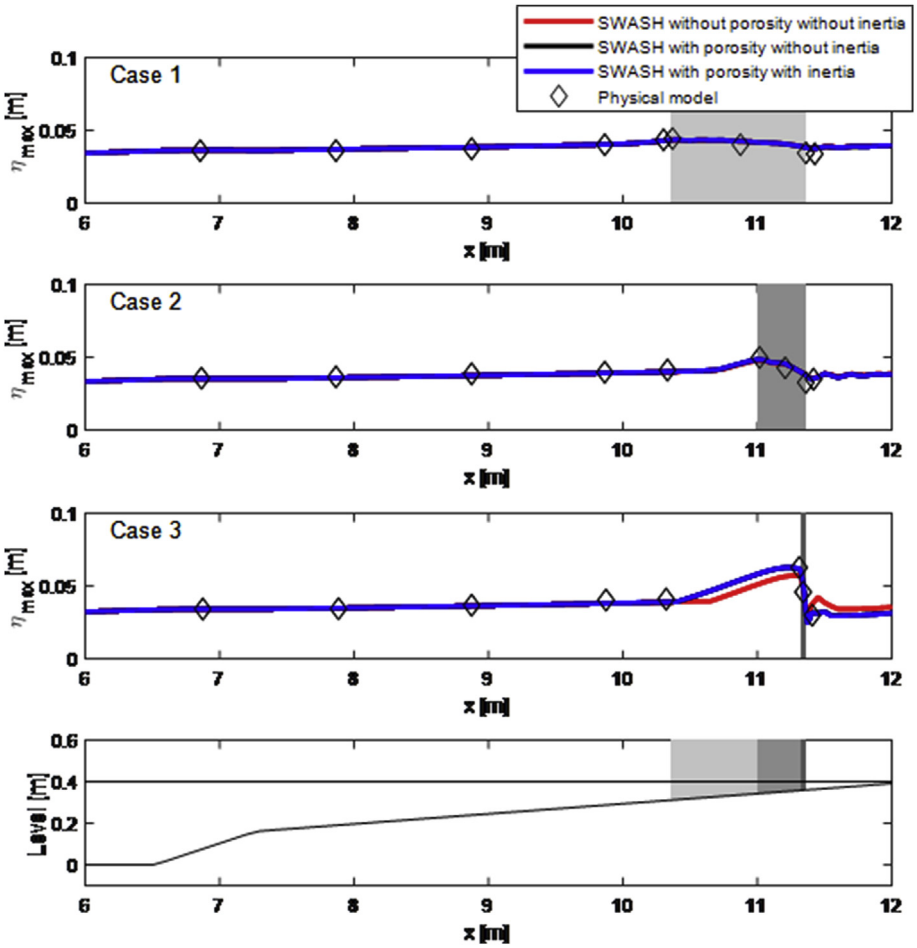

Fig. 10. SWASH modeling results and physical model data from Iimura and Tanaka (2012). The shaded area in each subplot indicates the vegetation patches. For cases 1 to 3, the tested N_v= 462, 1283 and 11,547 stems/m^2, respectively.

show that the run with both porosity and inertia effects fits better with the measurements. The gradual reduction of the wave height inside the vegetation canopy as well as the reflection at the canopy edge are well reproduced by such run. The run without either effect leads to overestimation of wave height inside the vegetation field. The run with porosity but no inertia effect has lower wave height at the vegetation edge and inside of the vegetation field. The reasons of the different model performances can be better explored in the following numerical experiment using the SWASH vegetation model in the next section.

The importance of porous and inertia effects relies on canopy porosity. Even with the same value of frontal vegetation area per canopy volume (i.e. , $N_v * b_v$), the canopy porosity (n = 1-ϕ) and associated porosity (and inertia) effects are different. Thus, we conduct a numerical experiment to test three canopies with identical $N_v * b_v$ but different porosities (Table 2). The case "poro049" with lowest canopy porosity (0.49) is relevant in reality, as porosity can be as low as 0.35 in constructed coastal wetlands (Serra et al., 2004). Low porosity may also be found in recent projects using porous brushwood groin for wave dissipation and creation of mangrove nurseries (Lucas, 2017) (Fig. 1c). The tested vegetation was placed on a slope at x = 11.5–15 m and was always emergent, as shown in Fig. 12 (bottom panel). The added-mass coefficient $C_m = 1$ was applied (Nepf, 2011).

The modeling results show that as the porosity decreased (increased ϕ) the difference induced by porosity and inertia effects became more apparent (Fig. 12). Overall, when both porosity and inertia effects are included, the wave dissipation is higher than in cases without either of these effects. These results also demonstrated that even with the same value of $N_v * b_v$, the porosity can still be different and its effect on wave transmission can be substantial.

When the porosity effect is included, wave reflection can be observed, similar to Arnaud et al. (2017). Because of the reflection (energy being reflected back in the opposite direction of the incident wave), wave-energy transmission through the vegetation field is reduced, i.e., there is reduced wave height within and behind the vegetation patches. This shows that the wave-reduction capacity of a low-porosity vegetation field (high ϕ) can be underestimated if the porosity effect is neglected.

When the inertia effect is included, the wave height within and behind the vegetation patch increases, i.e., there is reduced wave dissipation (Fig. 12). Such a reduction becomes more obvious with reduced porosity (increased ϕ). In previous theoretical (e.g., Méndez and Losada (2004)) and spectral domain models (e.g., Suzuki et al. (2012)), inertia force-oriented wave dissipation was zero, since the time integration of the work done by the inertia force was zero. Note that these previous models are based on first-order wave theory (i.e., there is no mass transport velocity). In a time-domain model (e.g., this study), we can calculate inertia force-oriented wave dissipation more accurately using time-dependent ζ and velocity. Eventually, the integration becomes non-zero.

Wave dissipation related to the inertia term over one wave period is expressed as

$$\varepsilon_{x\_inertia} = \overline{\int_{-d}^{\zeta} F_{x\_inertia}\, u\, dz} = \frac{1}{T}\int_{0}^{T}\int_{-d}^{\zeta} F_{x\_inertia} u\, dzdt \tag{15}$$

Assuming that vegetation is emergent, the wave dissipation is

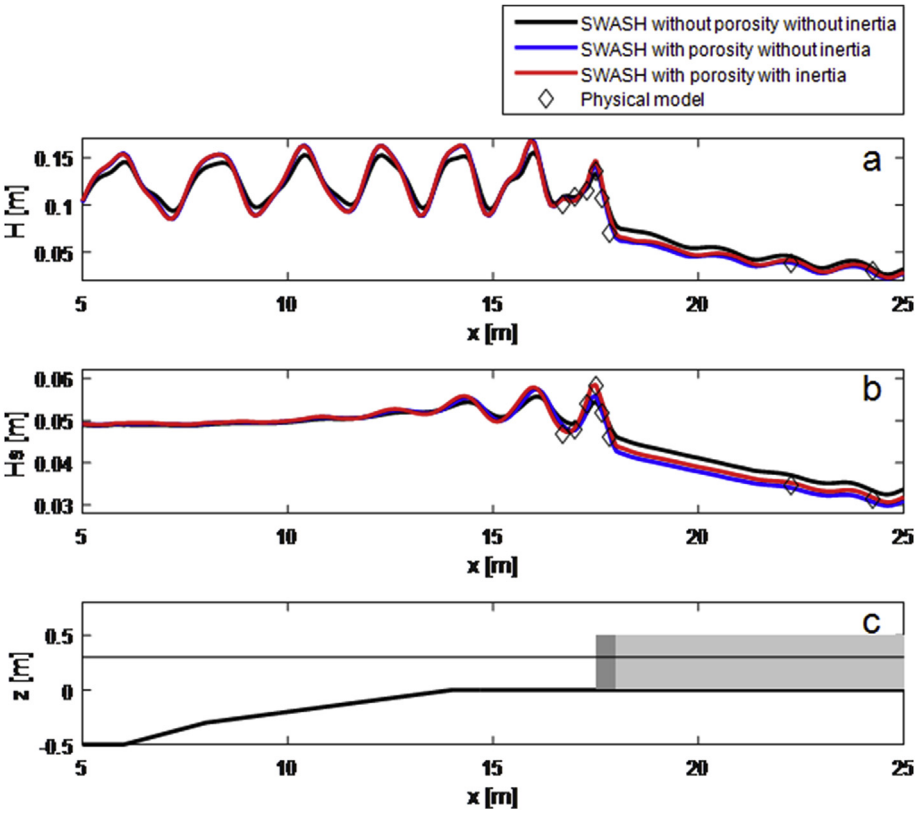

Fig. 11. SWASH modeling results of regular (plane a) and irregular (plane b) wave cases in comparison with the physical model data conducted in the Fluid Mechanics Laboratory at Delft University of Technology. The physical model setup is shown in panel c with a vegetation patch at x = 17.5 m–26.15 m.

Table 2
SWASH model runs with the same value of $N_v * b_v$, but different canopy porosity.

Case name	h (m)	b_v (m)	N_v (stems/m^2)	$N_v * b_v$	C_D	Porosity	ϕ
No veg	0	0	0	0	0	1	0
poro097	1	0.0032	3182	10.18	1.7	0.97	0.03
poro074	1	0.032	318	10.18	1.7	0.74	0.26
poro049	1	0.064	159	10.18	1.7	0.49	0.51

$$\varepsilon_{x\_inertia} = \frac{1}{T}\int_0^T \rho(1 + C_m)\frac{\pi}{4}b_v^2 N_v h(t)\frac{\partial u(t)}{\partial t}u(t)dt. \quad (16)$$

In the above Eq. (16), the time-varying term $h(t)\frac{\partial u(t)}{\partial t}u(t)$ is the key component, which may lead to non-zero wave energy dissipation under realistic conditions when water level, velocity, and acceleration are influenced by vegetation. The constant term $\rho C_M \frac{\pi}{4} b_v^2 N_v$ is clearly related to the porosity. The inertia effect can be expected to be more apparent with lower porosity (denser vegetation).

To find the reason for reduced wave dissipation with an inertia effect, modeled ζ, u, a (i.e. , $\frac{\partial u(t)}{\partial t}$), and wave dissipation due to inertia force were investigated over time (Fig. 13). Due to the asymmetric time series of ζ, u, and a, the wave dissipation was negative for most of the modeling period. This explains the reduced wave dissipation when an inertia effect is included. According to Eq. (16), this reduction can be more important with lower porosity (greater ϕ), which is confirmed by our modeling results (Fig. 13).

5. Discussion and conclusions

In the present study, we represent a new wave-vegetation model implemented in SWASH. The implementation of the drag force (induced by vertical cylinders) is validated against established analytical and numerical models (Cao et al., 2015; Méndez and Losada, 2004) and laboratory measurements (Wu et al., 2011). It has been shown that the modeled wave reduction is in good agreement with existing models and measurements. Even in the submerged-vegetation condition, wave dissipation is reproduced well by means of multi-layer calculation, which is not included in depth-integrated models. Additionally, the implementation of the porosity effect is also validated against physical model data in terms of the maximum water level in and around vegetation areas (Iimura and Tanaka, 2012). The newly-developed vegetation model in SWASH can properly simulate these important processes in wave propagation over a vegetation field.

Extended from existing models, the vegetation model in SWASH can simulate horizontal vegetation cylinders as well as porosity and inertia effects. Our modeling results show that these three newly-included effects can play important roles in wave propagation over vegetation fields, especially when the vegetation density (i.e., ϕ) is high. Horizontal vegetation cylinders are relevant in cases with dense, complex mangrove roots (Ohira et al., 2013; Kamal et al., 2014) and permeable groins constructed from horizontal brushwood (Lucas, 2017) (Fig. 1). The additional vertical drag force (F_z) acting on horizontal cylinders can be important when the waves are short (Fig. 9). For simplicity, the tested vegetation cylinders were either vertical or horizontal. However, in nature, mangroves are composed of both vertical and horizontal roots with complex patterns (Ohira et al., 2013; Kamal et al., 2014). For a better schematization of natural vegetation structures in numerical models, new image-processing techniques can automatically determine forest architecture (Kamal et al., 2014), which is worthy of future exploration. Nonetheless, the current vegetation model in SWASH is capable of describing non-isotropic feature of vegetation canopies, which has paved the way toward refined simulation of real mangrove root systems. It is noted that using the porous media approach with suitable tuning of empirical porous media coefficients (i.e. laminar friction loss and turbulent friction loss), similar wave

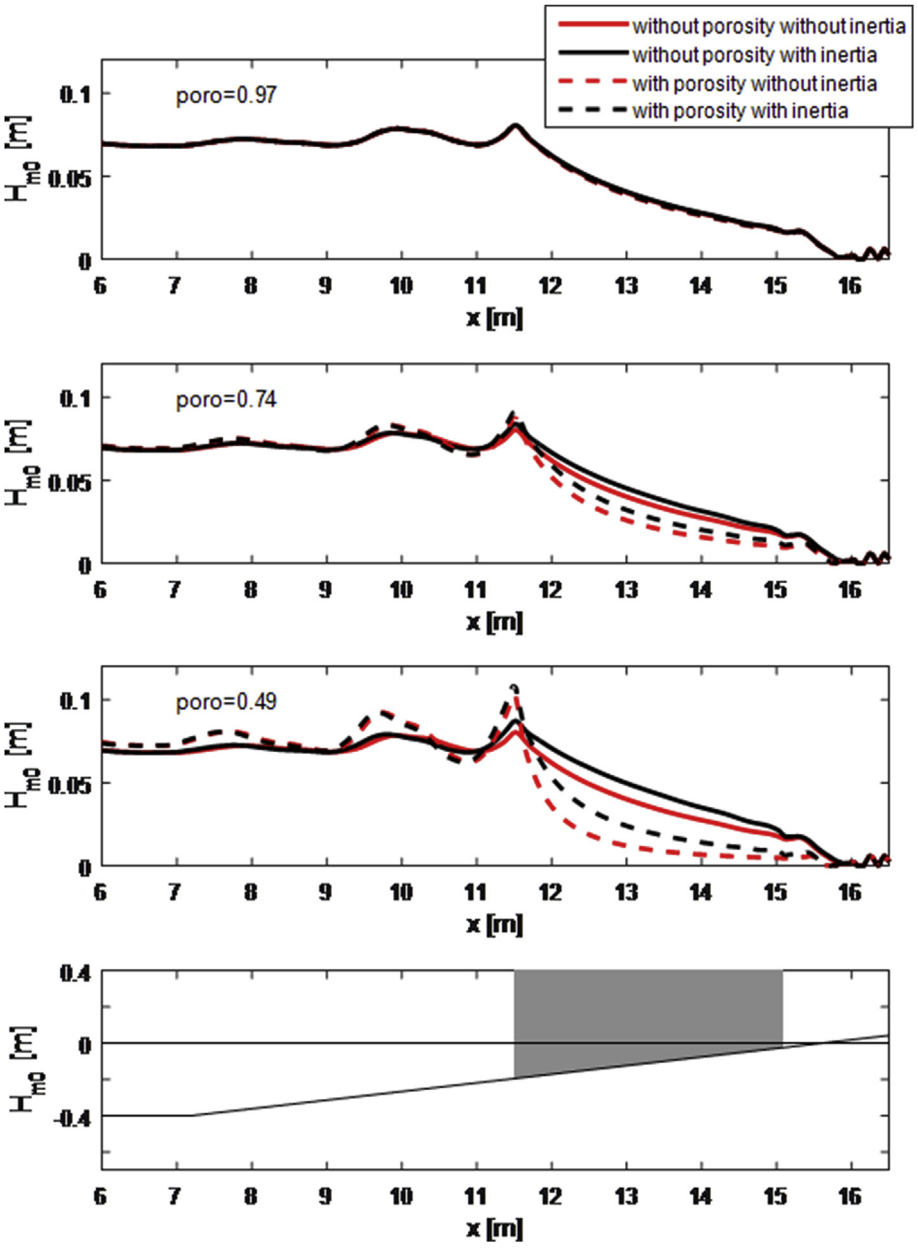

Fig. 12. Spatial distribution of H_s in tests that include or exclude porosity and/or inertia effects. The top three panels show tests with different porosity. The bottom panel shows the model setup with tested vegetation located on a slope at x = 11.5 to 15. The still wave level is at y = 0.

dissipation pattern can be obtained as the current implementation. However, the new model can facilitate the assessment of wave dissipation in real vegetation fields, which appears to be a more straightforward approach.

Our modeling results have also highlighted the relevance of porosity effects in flood-risk assessment. Essentially, flooding risks are related to both maximum water level and incident wave height. Our modeling results show that both are influenced by vegetation porosity, especially when vegetation density (ϕ) is high. Interestingly, there seems to be a trade-off related to the construction of dense vegetation fields for nature-based coastal defense. On one hand, the low porosity (high ϕ) induces wave reflection. Thus, it reduces the wave energy flux passing a vegetation field, and indirectly promotes its wave-reduction efficiency. On the other hand, the low porosity may cause local increases of the maximum water level due to wave run-up, which is highly undesirable for flood defense. A general management implication that can be derived from these results is that it is important to include the vegetation-porosity effect when designing nature-based coastal-defense projects, and well-defined design conditions should be regarded as a prerequisite to optimize the wave-damping capacity of vegetation without causing large increases of the maximum water level.

Our results further show that inertia force can be important when wave nonlinearity is high in dense vegetation field (high ϕ) (Figs. 11 and 12). Due to the asymmetric wave orbital velocity in shallow coastal vegetation areas, inertial force leads to negative energy dissipation that reduces the wave-damping capacity of vegetation. The effect of inertia force is small when the vegetation is not dense enough (say $\phi < 0.2$), and it increases gradually with vegetation density as indicated by Fig. 12. This probably explains why the effect of inertia force is often regarded negligible in previous studies (Maza et al., 2015). Our results show that neglecting the inertia effect may lead to overestimation of the wave-damping capacity of high-density vegetation fields. However, due to the reduced wave-energy transmission in vegetation areas, porosity effects can compensate for the negative energy dissipation induced by

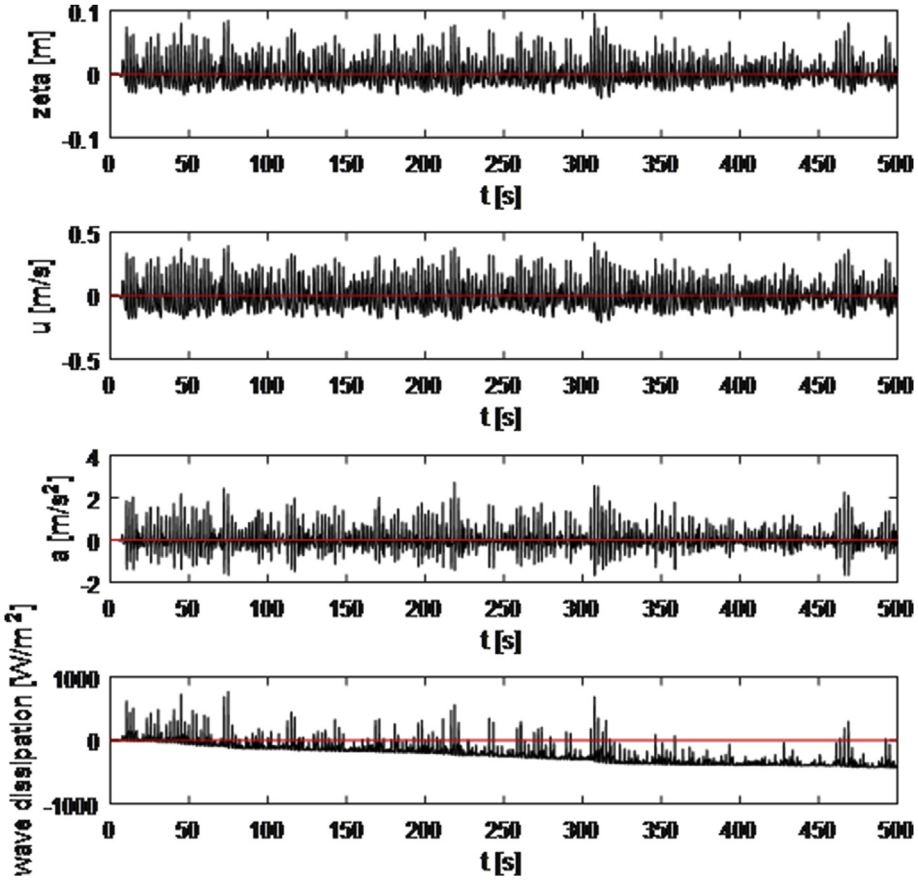

Fig. 13. Time series of ζ, u, a (i.e. , $\frac{\partial u(t)}{\partial t}$), and wave dissipation due to inertia force at x = 12 m (see bottom panel of Fig. 12).

inertia effects. The overall wave damping is enhanced when both inertia and porosity effects are considered, as compared to common simulations in previous modeling studies with neither effect.

Besides the inclusion of the additional inertia and porosity effects in the SWASH model, the strengths of the vegetation model in SWASH also lie in its computational efficiency, open-source nature, and capacity to model a variety of other processes like wave breaking, infragravity waves, suspended sediment transport, overtopping (Rijnsdorp et al., 2014; Suzuki et al., 2017; Zijlema et al., 2011). These processes ensure good representation of waves over vegetation fields and possibilities of conducting more comprehensive modeling studies including, e.g., nutrient loading and sediment dynamics. Compared to the SWAN vegetation module that can only handle narrow-banded random waves (Suzuki et al., 2012), the current model does not depend on the wave spectrum shape, as it is a time-domain model and wave dissipation is calculated at each time step. Therefore, the current model can calculate wave dissipation under any wave spectrum shape. Additionally, as mentioned above, this model automatically accounts for nonlinear effects, which is regarded as an advantage, as coastal wetlands are normally located in shallow zones with relatively strong nonlinear effects.

A few aspects of the SWASH wave-vegetation model require further study. For example, vegetation flexibility is not included. Flexibility has been noted as an important quality in a number of modeling studies (Dijkstra and Uittenbogaard, 2010; Maza et al., 2013). To accurately account for it, the model must specify the relative velocity between the vegetation stems and water motion (Dijkstra and Uittenbogaard, 2010), or specify the effective blade length (Luhar and Nepf, 2016). Determining which approach is more suitable for the SWASH model requires further investigation and validation with experiments (Sanchez-Gonzalez et al., 2011; Koftis et al., 2013). Additionally, recent studies have shown that current-wave interaction can influence the wave-dissipation rate in vegetation fields (Hu et al., 2014; Losada et al., 2016). As the SWASH model is based on nonlinear shallow-water equations, it can directly account for current-wave interactions, but proper simulations require more measuring data of the in-canopy flow field and insights on the vegetation drag coefficient in combined wave-current conditions. Finally, one should be cautious about the number of vertical layers applied in a simulation. A one-layer application may lead to large errors in cases with submerged vegetation and short waves. In these cases, multiple vertical layers should be applied. As the SWASH model can specify a non-equidistant layer distribution, users can define the layer thickness according to the ratio between the vegetation height and the water depth for efficient and accurate modeling.

In summary, we have developed a vegetation model within the structure of SWASH, which is an open-source non-hydrostatic wave-flow model (http://swash.sourceforge.net/). The effects of drag force by both vertical and horizontal vegetation cylinders, as well as inertia force and porosity, are explicitly included in the model. This new model is in good agreement with existing models, and it is also well validated against experimental data. The three new aspects we have identified have been demonstrated to be important, especially in dense vegetation fields. Thus, this new model offers an efficient and robust tool to quantify wave propagation and maximum water levels in coastal wetlands, and has great potential to serve nature-based coastal-defense projects, e.g., “Building with Nature” (Borsje et al., 2011; de Vriend et al., 2015; Vuik et al., 2016). Further research is needed to improve this model. Yet, the current model represents a solid advance toward refined simulation of wave propagation in vegetation fields.

Acknowledgements

We thank the two anonymous reviewers for their constructive

comments. The new vegetation model described in this paper is available in the SWASH open source code (http://swash.sourceforge.net). The authors gratefully acknowledge financial support of the National Natural Science Foundation of China (No. 51609269), the Joint Research Project NSFC (No. 51761135022) – NWO (No. ALWSD.2016.026) – EPSRC (No. EP/R024537/1): Sustainable Deltas and NSFC grants (No. 51520105014 and No. 41771095). We thank Patrick Lucas for providing photos of mangroves and permeable brushwood groin.

Appendix. Theoretical model on wave dissipation by horizontal vegetation cylinders in shallow water

The random wave transformation model in vertical cylinders for a flat bottom by Mendez and Losada (2004) is expressed as

$$H_{rms} = \frac{H_{rms,o}}{1 + \tilde{\beta}x} \tag{A.1}$$

With

$$\tilde{\beta} = \frac{1}{3\sqrt{\pi}} C_D b_v N_v H_{rms,o} k \frac{\sinh^3(k\alpha d) + 3\sinh(k\alpha d)}{\{\sinh(2kd) + 2kd\}\sinh(kd)} \tag{A.2}$$

where $H_{rms,o}$ is the root mean square wave height at the wave boundary, x = 0.

Wave dissipation by horizontal vegetation cylinders (transverse direction to the waves), which is contributed by the work done by the drag force acting in both the horizontal and vertical directions (Fig. 2). Thus, the time-averaged rate of energy dissipation per unit area over the entire height of vegetation or brushwood groins in shallow water is

$$\varepsilon_v = \varepsilon_{vx} + \varepsilon_{vz} = \overline{\int_{-d}^{-d+\alpha d} (F_x u + F_z w) dz} = \overline{\int_{-d}^{-d+\alpha d} \frac{1}{2}\rho C_D b_v N_v (|u|u^2 + |w|w^2) dz} \tag{A.3}$$

where u is the horizontal wave orbital velocity,

$$u = \frac{H}{2}\frac{gk}{\sigma}\frac{\cosh\{k(d+z)\}}{\cosh(kd)}\cos(kx - \sigma t) \tag{A.4}$$

and w is the vertical wave orbital velocity,

$$w = \frac{H}{2}\frac{gk}{\sigma}\frac{\sinh\{k(d+z)\}}{\cosh(kd)}\sin(kx - \sigma t) \tag{A.5}$$

The total time-averaged rate of energy dissipation per unit area ε_v in regular waves is

$$\varepsilon_v = \frac{2}{3\pi}\rho C_D b_v N_v \left(\frac{gk}{2\sigma}\right)^3 \frac{sinh^3(k\alpha d) + 3\sinh(k\alpha d) + cosh^3(k\alpha d) - 3\cosh(k\alpha d) + 2}{3k\ cosh^3(kd)} H^3 \tag{A.6}$$

Using the above equation, the conservation of energy equation can be rewritten as

$$\frac{\partial H^2}{\partial x} = -A_0 H^3 \tag{A.7}$$

where

$$A_0 = \frac{8}{9\pi} C_D b_v N_v k \frac{sinh^3(k\alpha d) + 3\sinh(k\alpha d) + cosh^3(k\alpha d) - 3\cosh(k\alpha d) + 2}{\{\sinh(2kd) + 2kd\}\ sinh(kd)} \tag{A.8}$$

Solving the linear differential equation and assuming that the wave height at the seaward edge of the vegetation field is H_0, we obtain

$$\frac{H}{H_0} = \frac{1}{1 + \beta x} = K_v \tag{A.9}$$

where K_v is defined as the damping coefficient (Méndez and Losada, 2004) and β is:

$$\beta = \frac{4}{9\pi} C_D b_v N_v H_o k \frac{\sinh^3(k\alpha d) + 3\sinh(k\alpha d) + \cosh^3(k\alpha d) - 3\cosh(k\alpha d) + 2}{\{\sinh(2kd) + 2kd\}\sinh(kd)} \tag{A.10}$$

Following Mendez and Losada (2004), when encountering random waves with a Rayleigh distribution, the total time-averaged rate of energy dissipation per unit area $<\varepsilon_v>$ is

$$<\varepsilon_v> = \frac{1}{2\sqrt{\pi}}\rho C_D b_v N_v \left(\frac{gk}{2\sigma}\right)^3 \frac{\sinh^3(k\alpha d) + 3\sinh(k\alpha d) + \cosh^3(k\alpha d) - 3\cosh(k\alpha d) + 2}{3k\ \cosh^3(kd)} H_{rms}^3 \tag{A.11}$$

Finally, $\tilde{\beta}$ for the horizontal vegetation cylinders is expressed as

$$\tilde{\beta} = \frac{1}{3\sqrt{\pi}} C_D b_v N_v H_{rms,o} k \frac{\sinh^3(k\alpha d) + 3\sinh(k\alpha d) + \cosh^3(k\alpha d) - 3\cosh(k\alpha d) + 2}{\{\sinh(2kd) + 2kd\}\sinh(kd)} \tag{A.12}$$

Appendix A. Supplementary data

Supplementary data to this article can be found online at https://doi.org/10.1016/j.coastaleng.2019.03.011.

References

Arkema, K.K., Guannel, G., Verutes, G., Wood, S.A., Guerry, A., Ruckelshaus, M., Kareiva, P., Lacayo, M., Silver, J.M., 2013. Coastal habitats shield people and property from sea-level rise and storms. Nat. Clim. Change 3, 913–918. https://doi.org/10.1038/nclimate1944.

Arnaud, G., Rey, V., Touboul, J., Sous, D., Molin, B., Gouaud, F., 2017. Wave propagation through dense vertical cylinder arrays: interference process and specific surface effects on damping. Appl. Ocean Res. 65, 229–237. https://doi.org/10.1016/j.apor.2017.04.011.

Asano, T., Tsutsui, S., Sakai, T., 1988. Wave damping characteristics due to seaweed. In: Proceedings of 35th Coastal Engineering Conference in Japan. Presented at the 35th Coastal Engineering Conference in Japan. Japan Society of Civil Engineers.

Augustin, L.N., Irish, J.L., Lynett, P., 2009. Laboratory and numerical studies of wave damping by emergent and near-emergent wetland vegetation. Coast. Eng. 56, 332–340.

Balke, T., Bouma, T.J., Horstman, E.M., Webb, E.L., Erftemeijer, P.L.A., Herman, P.M.J., 2011. Windows of opportunity: thresholds to mangrove seedling establishment on tidal flats. Mar. Ecol. Prog. Ser. 440, 1–9.

Borsje, B.W., van Wesenbeeck, B.K., Dekker, F., Paalvast, P., Bouma, T.J., van Katwijk, M.M., de Vries, M.B., 2011. How ecological engineering can serve in coastal protection. Ecol. Eng. 37, 113–122.

Bouma, T.J., van Belzen, J., Balke, T., Zhu, Z., Airoldi, L., Blight, A.J., Davies, A.J., Galvan, C., Hawkins, S.J., Hoggart, S.P.G., Lara, J.L., Losada, I.J., Maza, M., Ondiviela, B., Skov, M.W., Strain, E.M., Thompson, R.C., Yang, S., Zanuttigh, B., Zhang, L., Herman, P.M.J., 2014. Identifying knowledge gaps hampering application of intertidal habitats in coastal protection: opportunities & steps to take. Coast. Eng. 87, 147–157. https://doi.org/10.1016/j.coastaleng.2013.11.014.

Burcharth, H.F., Andersen, O.K., 1995. On the one-dimensional steady and unsteady porous flow equations. Coast. Eng. 24, 233–257. https://doi.org/10.1016/0378-3839(94)00025-S.

Cao, H., Feng, W., Hu, Z., Suzuki, T., Stive, M.J.F., 2015. Numerical modeling of vegetation-induced dissipation using an extended mild-slope equation. Ocean Eng. 110, 258–269. https://doi.org/10.1016/j.oceaneng.2015.09.057.

Chen, H., Ni, Y., Li, Y., Liu, F., Ou, S., Su, M., Peng, Y., Hu, Z., Uijttewaal, W., Suzuki, T., 2018. Deriving vegetation drag coefficients in combined wave-current flows by calibration and direct measurement methods. Adv. Water Resour. 122, 217–227. https://doi.org/10.1016/j.advwatres.2018.10.008.

Chen, X., Chen, Q., Zhan, J., Liu, D., 2016. Numerical simulations of wave propagation over a vegetated platform. Coast. Eng. 110, 64–75. https://doi.org/10.1016/j.coastaleng.2016.01.003.

Cuc, N.T.K., Suzuki, T., De, R.V.S., Hai, H., 2015. Modelling the impacts of mangrove vegetation structure on wave dissipation in Ben Tre Province, Vietnam, under different climate change scenarios. J. Coast. Res. 31, 340–347. https://doi.org/10.2112/JCOASTRES-D-12-00271.1.

Dalrymple, R., Kirby, J., Hwang, P., 1984. Wave diffraction due to areas of energy dissipation. J. Waterw. Port, Coast. Ocean Eng. 110, 67–79. https://doi.org/10.1061/(ASCE)0733–950X(1984)110:1(67).

de Vriend, H.J., van Koningsveld, M., Aarninkhof, S.G.J., de Vries, M.B., Baptist, M.J., 2015. Sustainable hydraulic engineering through building with nature. J. Hydro-Environ. Res. 9, 159–171. https://doi.org/10.1016/j.jher.2014.06.004.

Dijkstra, J.T., Uittenbogaard, R.E., 2010. Modeling the interaction between flow and highly flexible aquatic vegetation. Water Resour. Res. 46.

Furukawa, K., Wolanski, E., Mueller, H., 1997. Currents and sediment transport in mangrove forests. Estuar. Coast Shelf Sci. 44, 301–310. https://doi.org/10.1006/ecss.1996.0120.

Goda, Y., 2010. Random seas and design of maritime structures. In: Advanced Series on Ocean Engineering, third ed. World Scientific Publishing.

Hasselmann, K., Collins, J., 1968. Spectral dissipation of finite depth gravity waves due to turbulent bottom friction. J. Mar. Res. 26, 1–12.

Hu, Z., Suzuki, T., Zitman, T., Uijttewaal, W., Stive, M., 2014. Laboratory study on wave dissipation by vegetation in combined current-wave flow. Coast. Eng. 88, 131–142. https://doi.org/10.1016/j.coastaleng.2014.02.009.

Hu, Z., Van Belzen, J., Van Der Wal, D., Balke, T., Wang, Z.B., Stive, M., Bouma, T.J., 2015. Windows of opportunity for salt marsh vegetation establishment on bare tidal flats: the importance of temporal and spatial variability in hydrodynamic forcing. J. Geophys. Res. G Biogeosciences 120, 1450–1469. https://doi.org/10.1002/2014JG002870.

Huang, Z., Yao, Y., Sim, S.Y., Yao, Y., 2011. Interaction of solitary waves with emergent, rigid vegetation. Ocean Eng. 38, 1080–1088.

Iimura, K., Tanaka, N., 2012. Numerical simulation estimating effects of tree density distribution in coastal forest on tsunami mitigation. Ocean Eng. 54, 223–232. https://doi.org/10.1016/j.oceaneng.2012.07.025.

Jensen, B., Jacobsen, N.G., Christensen, E.D., 2014. Investigations on the porous media equations and resistance coefficients for coastal structures. Coast. Eng. 84, 56–72. https://doi.org/10.1016/j.coastaleng.2013.11.004.

Kamal, S., Lee, S.Y., Warnken, J., 2014. Investigating three-dimensional mesoscale habitat complexity and its ecological implications using low-cost RGB-D sensor technology. Methods Ecol. Evol. 5, 845–853. https://doi.org/10.1111/2041-210X.12210.

Karambas, T., Koftis, T., Prinos, P., 2016. Modeling of nonlinear wave attenuation due to vegetation. J. Coast. Res. 32, 142–152. https://doi.org/10.2112/JCOASTRES-D-14-00044.1.

Kobayashi, N., Raichle, A.W., Asano, T., 1993. Wave attenuation by vegetation. J. Waterw. Port Coast. Ocean Eng. - ASCE 119, 30–48.

Koftis, T., Prinos, P., Stratigaki, V., 2013. Wave damping over artificial Posidonia oceanica meadow: a large-scale experimental study. Coast. Eng. 73, 71–83. https://doi.org/10.1016/j.coastaleng.2012.10.007.

Li, C.W., Yan, K., 2007. Numerical investigation of wave - current - vegetation interaction. J. Hydraul. Eng. 133, 794–803. https://doi.org/10.1061/(ASCE)0733-9429(2007)133:7(794).

Liu, P.L.-F., Chang, C.-W., Mei, C.C., Lomonaco, P., Martin, F.L., Maza, M., 2015. Periodic water waves through an aquatic forest. Coast. Eng. 96, 100–117. https://doi.org/10.1016/j.coastaleng.2014.11.002.

Losada, I.J., Maza, M., Lara, J.L., 2016. A new formulation for vegetation-induced damping under combined waves and currents. Coast. Eng. 107, 1–13. https://doi.org/10.1016/j.coastaleng.2015.09.011.

Lucas, P., 2017. Measuring and Modelling Wave Damping by Permeable Groins (Master Thesis). Universität Stuttgart, Stuttgart.

Luhar, M., Nepf, H.M., 2016. Wave-induced dynamics of flexible blades. J. Fluids Struct. 61, 20–41. https://doi.org/10.1016/j.jfluidstructs.2015.11.007.

Ma, G., Kirby, J.T., Su, S.-F., Figlus, J., Shi, F., 2013. Numerical study of turbulence and wave damping induced by vegetation canopies. Coast. Eng. 80, 68–78. https://doi.org/10.1016/j.coastaleng.2013.05.007.

Mariotti, G., Fagherazzi, S., 2010. A numerical model for the coupled long-term evolution of salt marshes and tidal flats. J. Geophys. Res. F Earth Surf. 115.

Maza, M., Lara, J.L., Losada, I.J., 2016. Solitary wave attenuation by vegetation patches. Adv. Water Resour. 98, 159–172. https://doi.org/10.1016/j.advwatres.2016.10.021.

Maza, M., Lara, J.L., Losada, I.J., 2015. Tsunami wave interaction with mangrove forests: a 3-D numerical approach. Coast. Eng. 98, 33–54. https://doi.org/10.1016/j.coastaleng.2015.01.002.

Maza, M., Lara, J.L., Losada, I.J., 2013. A coupled model of submerged vegetation under oscillatory flow using Navier-Stokes equations. Coast. Eng. 80, 16–34. https://doi.org/10.1016/j.coastaleng.2013.04.009.

Mazda, Y., Wolanski, E., King, B., Sase, A., Ohtsuka, D., Magi, M., 1997. Drag force due to vegetation in mangrove swamps. Mangroves Salt Marshes 1, 193–199. https://doi.org/10.1023/A:1009949411068.

Mei, C.C., Chan, I.-C., Liu, P.L.-F., Huang, Z., Zhang, W., 2011. Long waves through emergent coastal vegetation. J. Fluid Mech. 687, 461–491. https://doi.org/10.1017/jfm.2011.373.

Méndez, F.J., Losada, I.J., 2004. An empirical model to estimate the propagation of random breaking and nonbreaking waves over vegetation fields. Coast. Eng. 51, 103–118.

Méndez, F.J., Losada, I.J., Losada, M.A., 1999. Hydrodynamics induced by wind waves in a vegetation field. J. Geophys. Res. C Ocean. 104, 18383–18396.

Möller, I., Kudella, M., Rupprecht, F., Spencer, T., Paul, M., van Wesenbeeck, B.K., Wolters, G., Jensen, K., Bouma, T.J., Miranda-Lange, M., Schimmels, S., 2014. Wave attenuation over coastal salt marshes under storm surge conditions. Nat. Geosci. 7, 727–731. https://doi.org/10.1038/ngeo2251.

Möller, I., Spencer, T., French, J.R., Leggett, D.J., Dixon, M., 1999. Wave transformation over salt marshes: a field and numerical modelling study from north Norfolk, England. Estuar. Coast Shelf Sci. 49, 411–426. https://doi.org/10.1006/ecss.1999.0509.

Morison, J.R., O'Brien, M.P., Johnson, J.W., Schaaf, S.A., 1950. The Force Exerted by Surface Waves on Piles.

Nepf, H.M., 2011. Flow over and through biota. In: Wolanski, E., McLusky, D. (Eds.), Treatise on Estuarine and Coastal Science. Academic Press, Waltham, pp. 267–288.

Ohira, W., Honda, K., Nagai, M., Ratanasuwan, A., 2013. Mangrove stilt root morphology modeling for estimating hydraulic drag in tsunami inundation simulation. Trees Struct. Funct. 27, 141–148. https://doi.org/10.1007/s00468-012-0782-8.

Rijnsdorp, D.P., Smit, P.B., Zijlema, M., 2014. Non-hydrostatic modelling of infragravity waves under laboratory conditions. Coast. Eng. 85, 30–42. https://doi.org/10.1016/j.coastaleng.2013.11.011.

Sanchez-Gonzalez, J.F., Sanchez-Rojas, V., Memos, C.D., 2011. Wave attenuation due to Posidonia oceanica meadows. J. Hydraul. Res. 49, 503–514. https://doi.org/10.1080/00221686.2011.552464.

Serra, T., Fernando, H.J.S., Rodriguez, R.V., 2004. Effects of emergent vegetation on lateral diffusion in wetlands. Water Res. 38, 139–147. https://doi.org/10.1016/j.watres.2003.09.009.

Suzuki, T., Altomare, C., Veale, W., Verwaest, T., Trouw, K., Troch, P., Zijlema, M., 2017. Efficient and robust wave overtopping estimation for impermeable coastal structures in shallow foreshores using SWASH. Coast. Eng. 122, 108–123. https://doi.org/10.1016/j.coastaleng.2017.01.009.

Suzuki, T., Zijlema, M., Burger, B., Meijer, M.C., Narayan, S., 2012. Wave dissipation by vegetation with layer schematization in SWAN. Coast. Eng. 59, 64–71.

Tang, J., Shen, S., Wang, H., 2015. Numerical model for coastal wave propagation through mild slope zone in the presence of rigid vegetation. Coast. Eng. 97, 53–59. https://doi.org/10.1016/j.coastaleng.2014.12.006.

Temmerman, S., Meire, P., Bouma, T.J., Herman, P.M.J., Ysebaert, T., De Vriend, H.J., 2013. Ecosystem-based coastal defence in the face of global change. Nature 504, 79–83. https://doi.org/10.1038/nature12859.

van Loon-Steensma, J.M., Hu, Z., Slim, P.A., 2016. Modelled impact of vegetation heterogeneity and salt-marsh zonation on wave damping. J. Coast. Res. 32, 241–252. https://doi.org/10.2112/JCOASTRES-D-15-00095.1.

van Rooijen, A.A., McCall, R.T., de Vries, J.S.M. van T., van Dongeren, A.R., Reniers, A.J.H.M., Roelvink, J.A., 2016. Modeling the effect of wave-vegetation interaction on wave setup. J. Geophys. Res.-Oceans 121, 4341–4359. https://doi.org/10.1002/2015JC011392.

Vuik, V., Jonkman, S.N., Borsje, B.W., Suzuki, T., 2016. Nature-based flood protection: the efficiency of vegetated foreshores for reducing wave loads on coastal dikes. Coast.

Eng. 116, 42–56. https://doi.org/10.1016/j.coastaleng.2016.06.001.
Wu, W., Ozeren, Y., Wren, D., Chen, Q., Zhang, G., Holland, M., Ding, Y., Kuiry, S., Zhang, M., Jadhave, R., Chatagnier, J., Chen, Y., Gordji, L., 2011. Phase I Report for SERRI Project No. 80037: Investigation of Surge and Wave Reduction by Vegetation (Report No. 80037– 01). Oak Ridge National Laboratory, Oak Ridge, Tennessee.
Yang, Z., Tang, J., Shen, Y., 2018. Numerical study for vegetation effects on coastal wave propagation by using nonlinear Boussinesq model. Appl. Ocean Res. 70, 32–40. https://doi.org/10.1016/j.apor.2017.09.001.
Yao, P., Chen, H., Huang, B., Tan, C., Hu, Z., Ren, L., Yang, Q., 2018. Applying a new force-velocity synchronizing algorithm to derive drag coefficients of rigid vegetation in oscillatory flows. Water 10, 906. https://doi.org/10.3390/w10070906.
Zijlema, M., Stelling, G., Smit, P., 2011. SWASH: an operational public domain code for simulating wave fields and rapidly varied flows in coastal waters. Coast. Eng. 58, 992–1012.